Edinburgh Research Explorer

Stability analysis of ecomorphodynamic equations

OPEN ACCESS

[1] STABILITY ANALYSIS OF
[2] ECOMORPHODYNAMIC EQUATIONS

F. Bärenbold,[1] B. Crouzy,[1], and P. Perona,[1]

[1]Group AHEAD, Institute of

Environmental Engineering, EPFL-ENAC,

Station 2, 1015 Lausanne, CH.

Abstract.   In order to shed light on the influence of riverbed vegetation

on river morphodynamics, we perform a linear stability analysis on a min-

imal model of vegetation dynamics coupled with classical one- and two-dimensional

Saint-Venant-Exner equations of morphodynamics. Vegetation is modeled

as a density field of rigid, non-submerged cylinders and affects flow via a rough-

ness change. Furthermore, vegetation is assumed to develop following a lo-

gistic dependence and may be uprooted by flow. First, we perform the sta-

bility analysis of the reduced one-dimensional framework. As a result of the

competitive interaction between vegetation growth and removal through up-

rooting, we find a domain in the parameter space where originally straight

rivers are unstable towards periodic longitudinal patterns. For realistic val-

ues of the sediment transport parameter, the dominant longitudinal wave-

length is determined by the parameters of the vegetation model. Bed topog-

raphy is found to adjust to the spatial pattern fixed by vegetation. Subse-

quently, the stability analysis is repeated for the two-dimensional framework,

where the system may evolve towards alternate or multiple bars. On a fixed

bed, we find instability towards alternate bars due to flow-vegetation inter-

action, but no multiple bars. Both alternate and multiple bars are present

on a movable, vegetated bed. Finally, we find that the addition of vegeta-

tion to a previously unvegetated riverbed favors instability towards alternate

bars and thus the development of a single course rather than braiding.

1. Introduction

River planform morphologies, like meandering and braiding, are the result of the inter-action between flow and sediment transport (see for example *Seminara* [2010] and refer-ences therein, or for an illustration Figures 1A and B) as well as of riparian vegetation dynamics. In particular, it is recognized that riparian vegetation affects river morphology through modification of the flow field [*Nepf*, 2012], increased bank strength [*Pollen and Simon*, 2005] and changes in erosion/sedimentation processes in the riverbed/floodplain (see *Gurnell et al.* [2012] or *Camporeale et al.* [2013], for a review).

Plant-flow interaction in rivers was favored by the emergence of plant roots in the Pale-ozoic and promoted new morphodynamic processes and morphological patterns. In turn, plant adaptation and feedback strengthening tremendously impacted landscape evolution (*Davies and Gibling* [2010] and *Gibling and Davies* [2012]). Today, the interaction dy-namics between riparian vegetation, flow and sediment is also thought to be crucial for instance in the formation of multiple bars and anabranching river patterns (see for exam-ple *Jansen and Nanson* [2010], or for an illustration Figures 1C and D).

The influence of riparian vegetation on river morphology/planform patterns has tradition-ally been investigated either by means of numerical simulations or by experiments. *Li and Millar* [2011] and *Nicholas et al.* [2013] modeled riparian vegetation as a parameter influ-encing bank strength and *Murray and Paola* [2003] used a rule-based approach to model vegetation-induced bank strengthening. In addition, *Crosato and Saleh* [2011] included vegetation flow resistance in a morphodynamic model. Common among these works is the conclusion that the presence of riparian vegetation encourages meandering while un-

45   vegetated rivers tend to braid. Furthermore, *Perucca et al.* [2007] modeled vegetation as

46   a function of distance to the river as well as its impact on bank stability and they ob-

47   served that meander form and wavelength change with respect to a non-vegetated river.

48   More recently, *Bertoldi et al.* [2014] developed a numerical model including vegetation

49   growth and uprooting dynamics to shed light on the effect of vegetation in the formation

50   of alternate bars. Experimental works include *Federici and Paola* [2003] on alternate bar

51   formation, *Coulthard* [2005] on sheltering that plants exert as passive porous obstacles,

52   *Tal and Paola* [2007] on the active role of vegetation colonization in favoring transition

53   from braided to single thread streams. Additionally, conceptual models have been used

54   to analyze the dynamics of specific rivers (see *Tooth and Nanson* [2000] for the Marshall

55   River and *Gurnell and Petts* [2006] for the Tagliamento River) and neural models [*Crouzy*

56   *et al.*, 2015] were used to obtain quantitative results.

57   Theoretical approaches based on linear stability analysis have been shown to predict in-

58   stability towards alternate or multiple bars on a movable riverbed (*Callander* [1969],

59   *Engelund and Skovgaard* [1973], *Parker* [1976] and *Colombini et al.* [1987]). A common

60   finding of these studies is that the key parameter in the formation of alternate bars or

61   multiple bars is the river's aspect ratio (halfwidth-to-depth ratio). Figure 2 shows a typi-

62   cal result of such a stability analysis. Note the presence of a lower threshold for the aspect

63   ratio separating stability from instability.

64   However, due to the very complex nature of the dynamic interactions between riparian

65   vegetation and sediment transport and flow, vegetation evolution was never taken into

66   account explicitly in a linear stability analysis. While the omission of vegetation may

67   be justified when looking at short timescales where riparian vegetation density does not

change much (and thus can be represented by a correction factor), this is not the case

for river pattern formation that occurs over much longer timescales and where vegetation

takes an active role in the process.

Extending the results of *Crouzy et al.* [2015], which focused on anabranching patterns, we

perform a systematic stability analysis of the model of *Perona et al.* [2014] modified to

include local positive effects due to the presence of vegetation. We first propose a mini-

mal model for riverbed vegetation dynamics including only logistic growth, local positive

feedback and mortality by means of uprooting and then couple it with a standard two-

dimensional framework for river morphodynamics (see *Federici and Seminara* [2003] for

example) in Section 2. Linear stability analysis is performed in order to identify regions

in the parameter space where instability towards periodic patterns exist (Section 3) and

the results are discussed in Section 4.

2. Modeling

2.1. Riverbed vegetation dynamics

We develop an analytical model for riverbed vegetation dynamics and discuss its validity for different conditions. Physical variables (Table 1) are written adopting a tilde (e.g. $\tilde{v}$) in order to distinguish them from dimensionless ones. Riverbed vegetation is modeled as rigid, non-submerged cylinders with constant radius and we call $\tilde{\phi}(\tilde{s}, \tilde{n}, \tilde{t})$ its density defined as number of plants per unit area of riverbed as a function of streamwise coordinate $\tilde{s}$, transverse coordinate $\tilde{n}$ and time $\tilde{t}$. Then, we write the rate of change of vegetation density as

$$\frac{\partial \tilde{\phi}}{\partial \tilde{t}} = \alpha_g' \tilde{\phi}(\tilde{\phi}_m - \tilde{\phi}) + D' \nabla^2 \tilde{\phi} - \alpha_d' \tilde{Y} \|\tilde{\mathbf{V}}\|^2 \tilde{\phi}. \tag{1}$$

Here, in the right hand side the first term represents logistic growth with α_g' the growth coefficient and $\tilde{\phi}_m$ the carrying capacity (logistic growth for riparian vegetation was used in *Camporeale and Ridolfi* [2006] for example). The second term is a diffusion term with diffusion coefficient D', which is a substantial novelty compared to the model of *Perona et al.* [2014]. This term indeed accounts for the fact that vegetation development is favored by existing neighboring vegetation (i.e. local positive feedback) by means of increased seed deposition and resprouting for example. According to *D'Odorico et al.* [2007] and *Crouzy et al.* [2015] such a local positive feedback can in general be represented by a diffusion term. Finally, the third term models negative feedback between flow and vegetation which results in vegetation removal by means of uprooting due to flow drag (Type I mechanism after *Edmaier et al.* [2011]). In this case, the rate of fluid mass that impacts on vegetation is proportional to the square of the stream velocity while the vegetation cross-section per cubic meter of river is proportional to water depth and vegetation density. While it would

Table 1. Summary of the variables used in this work

Name	Description
SV	Saint-Venant Model
SVE	Saint-Venant-Exner Model
SVV	Saint-Venant-Vegetation Model
SVEV	Saint-Venant-Exner-Vegetation Model

Name	Ddescription
$\tilde{\eta}(\eta)$	(a)dimensional bed elevation
$\chi_b(c_b)$	(a)dimensional bed roughness (Chézy)
$\tilde{s}(s)$	(a)dimensional streamwise coordinate
$\tilde{U}(U)$	(a)dimensional streamwise velocity
$k_s(\tilde{k}_s)$	(a)dimensional streamwise wavenumber
$\tilde{t}(t)$	(a)dimensional time
$\tilde{n}(n)$	(a)dimensional transverse coordinate
$\tilde{V}(V)$	(a)dimensional transverse velocity
$k_n(\tilde{k}_n)$	(a)dimensional transverse wavenumber
$\tilde{\phi}(\phi)$	(a)dimensional vegetation density
$\alpha_g(\nu_g)$	(a)dimensional vegetation growth coefficient
$D(\nu_D)$	(a)dimensional vegetation diffusion coefficient
$\alpha_d(\nu_d)$	(a)dimensional vegetation mortality coefficient
$\tilde{Y}(Y)$	(a)dimensional water depth
γ	ratio between morphodynamic and hydrodynamic timescale
c_v	adimensional vegetation roughness coefficient
β	aspect ratio
p	bed porosity
$\tilde{Q}_{s0}$	dimensional sediment transport rate under normal flow conditions
$\tilde{\phi}_m$	dimensional vegetation carrying capacity
$\tilde{t}_d$	drought period
a	empiricall parameter in sediment transport law
r	empiricall parameter in transverse slope term
$\tilde{t}_f$	flooding period
F_0	Froude number
g	gravitational acceleration
d	idealized vegetation diameter
d_{50}	median grain diameter
ρ_s	sediment density
δ	sediment transport deviation angle
k_{st}	Strickler roughness coefficient
χ	total Chézy roughness
m	bar order
$\tilde{t}_v$	vegetation period
c_D	vegetation Stokes coefficient
ρ	water density

seem reasonable to add a threshold below which root resistance prevents uprooting, *Perona et al.* [2012] found that there are always a certain number of plants with very shallow root depth. Assuming a linear relationship between flow drag and biomass removal, this results in a vegetation mortality rate directly proportional to the square of the stream velocity vector $\tilde{\mathbf{V}}$, to water depth $\tilde{Y}$ and to vegetation density through a coefficient α'_d.

Typically, large parts of a river's cross-section are only flooded during a limited amount of time per year thus allowing vegetation to colonize these surfaces during non-flooded periods. In contrast, during a flooding period vegetation growth is negligible compared to uprooting. This means that the different processes of vegetation evolution do not necessarily happen at the same time and therefore equation (1) needs to be modified in order to still be applicable for vegetation dynamics in natural streams. In fact, the difficulty to separate these processes in one single equation is the main reason why many models do not account for vegetation dynamics.

Assuming that the riverbed morphology and the vegetation cover do not change too much over a cycle flooding event - low flow interval, we can still use a description of the form of equation (1). This means that the vegetation cover is dense enough to not allow much more biomass to be produced and at the same time a large part of the vegetation is robust enough to outlive the flooding period. According to this assumption, the hydrograph may be divided into three periods: during the vegetation period $\tilde{t}_v$ vegetation grows and spreads, uprooting takes place during the flooding period $\tilde{t}_f$ and vegetation density is assumed to remain constant during the drought period $\tilde{t}_d$. We then assume that this succession is happening repeatedly with constant $\tilde{t}_v$, $\tilde{t}_d$ and $\tilde{t}_f$. In this way, the time from the start of one flooding event to the next one may be interpreted as a cycle whose length

125 is given by $\tilde{t}_d + \tilde{t}_v + \tilde{t}_f$ (see Figure 3 for illustration). As shown by *Crouzy et al.* [2015],

126 it is then possible to integrate the growth and diffusion processes into the flooding period

127 and thus to recover the constant and continuous flow assumption to end up with

$$\frac{\partial \tilde{\phi}}{\partial \tilde{t}} = \alpha_g \tilde{\phi}(\tilde{\phi} - \tilde{\phi}_m) + D\nabla^2 \tilde{\phi} - \alpha_d \tilde{Y} \|\tilde{\mathbf{V}}\|^2 \tilde{\phi}, \tag{2}$$

129 where $\alpha_g = \alpha'_g \frac{\tilde{t}_v}{\tilde{t}_d + \tilde{t}_v + \tilde{t}_f}$, $D = D' \frac{\tilde{t}_v}{\tilde{t}_d + \tilde{t}_v + \tilde{t}_f}$ and $\alpha_d = \alpha'_d \frac{\tilde{t}_f}{\tilde{t}_d + \tilde{t}_v + \tilde{t}_f}$. We can see that merging

130 together the different mechanisms results in a relative increase or decrease of the growth

131 and diffusion coefficients with respect to the uprooting coefficient depending on which

132 timescale dominates. Note that usually these timescales are very different. In the case of

133 the Marshall River (see *Tooth and Nanson* [2004]) and also for bar flooding in the Thur

134 River (see for example *Pasquale et al.* [2010]) the flooding period is very small compared

135 to the vegetation period and consequently, α_d is decreased while α_g and D are increased

136 to yield a regime where mutual feedback is possible.

137

2.2. Coupling with river morphodynamics

In this section, we couple the vegetation model developed in Section 2.1 with a model for flow and sediment dynamics in a straight, rectangular channel with constant width, movable bed and non-erodible banks (see *Blondeaux and Seminara* [1985] for curved channels). A scheme is depicted in Figure 4 showing the streamwise and transverse coordinates $\tilde{s}$ and $\tilde{n}$ to which we associate the velocity vector $\tilde{\mathbf{V}} = \{\tilde{U}, \tilde{V}\}$. We introduce also uniform (perturbed) bed elevation $\tilde{\eta}_0$ ($\tilde{\eta}$) and water depth $\tilde{Y}_0$ ($\tilde{Y}$) respectively. Furthermore, we assume the river bed to consist of non-cohesive, alluvial material of constant grain size on which vegetation is able to grow and the river width to be considerably larger than flow depth in order to be able to use a depth-averaged formulation. We then can write momentum balance, continuity for flow and sediment and vegetation dynamics in its dimensionless form as

$$\frac{\partial U}{\partial t} = -U\frac{\partial U}{\partial s} - V\frac{\partial U}{\partial n} - \frac{1}{F_0^2}\left[\frac{\partial Y}{\partial s} - \frac{\partial \eta}{\partial s}\right] - \beta\frac{\tau_s}{Y} \tag{3}$$

$$\frac{\partial V}{\partial t} = -U\frac{\partial V}{\partial s} - V\frac{\partial V}{\partial n} - \frac{1}{F_0^2}\left[\frac{\partial Y}{\partial n} - \frac{\partial \eta}{\partial n}\right] - \beta\frac{\tau_n}{Y} \tag{4}$$

$$\frac{\partial Y}{\partial t} = -\nabla \cdot (Y\mathbf{V}) \tag{5}$$

$$\frac{\partial \eta}{\partial t} = -\gamma\nabla \cdot (\|\mathbf{V}\|^3\{\cos\delta, \sin\delta\}) \tag{6}$$

$$\frac{\partial \phi}{\partial t} = \nu_g\phi(1 - \phi) + \nu_D\nabla^2\phi - \nu_d Y\|\mathbf{V}\|^2\phi, \tag{7}$$

where the physical variables were made dimensionless using the uniform flow conditions $\{\tilde{U}_0, \tilde{Y}_0, \tilde{\eta}_0, \tilde{B}_0\}$ with channel width $2\tilde{B}_0$. In order to recover physical quantities one needs to take $\{U, V\} = \tilde{U}_0^{-1}\{\tilde{U}, \tilde{V}\}$, $\{Y, \eta\} = \tilde{Y}_0^{-1}\{\tilde{Y}, \tilde{\eta}\}$, $\phi = \tilde{\phi}_m^{-1}\tilde{\phi}$, $\{s, n\} = \tilde{B}_0^{-1}\{\tilde{s}, \tilde{n}\}$ and $t = \tilde{U}_0\tilde{B}_0^{-1}\tilde{t}$. Then, $F_0 = \frac{\tilde{U}_0}{\sqrt{g\tilde{Y}_0}}$ with g the gravitational acceleration is the Froude number and $\beta = \frac{\tilde{B}_0}{\tilde{Y}_0}$ is the aspect ratio at normal flow. We use the Chézy formula as closure relation

159 for the momentum equations with total shear stress as $\tilde{\boldsymbol{\tau}} = \{\tilde{\tau}_s, \tilde{\tau}_n\} = \frac{g}{\chi^2}\|\tilde{\mathbf{V}}\|\{\tilde{U}, \tilde{V}\}$. The

160 total friction coefficient χ is then modified to account for vegetation-induced friction

161 (following *Baptist et al.* [2007]) to get

$$\chi = \sqrt{\frac{1}{\frac{1}{\chi_b^2} + \frac{c_D\, d\, \tilde{\phi}\tilde{Y}}{2g}}}, \tag{8}$$

163 with χ_b the bed friction coefficient which can be calculated by fixing the Strickler coefficient

164 k_s, c_D the vegetation's Stokes drag coefficient and d the vegetation diameter. We can

165 rewrite total bed shear stress as

$$\tilde{\boldsymbol{\tau}} = \{\tilde{\tau}_s, \tilde{\tau}_n\} = (c_b + c_v Y\phi)\|\tilde{\mathbf{V}}\|\{\tilde{U}, \tilde{V}\}, \tag{9}$$

167 with $c_b = \frac{g}{\chi_b^2}$ and $c_v = \frac{c_D d\tilde{\phi}_m\tilde{Y}_0}{2}$.

168 A second closure relation is needed for sediment continuity for which we assume bed load

169 transport only and thus use a power law in the form of $\tilde{\Phi} = a\|\tilde{\mathbf{V}}\|^3$ with a an empirical

170 parameter as was done by *Camporeale and Ridolfi* [2009]. Note that this relationship

171 between sediment transport rate and stream velocity is an approximation to the Meyer-

172 Peter/Müller formula used by *Colombini et al.* [1987] and *Federici and Seminara* [2003]

173 where the threshold is removed.

174 The sediment continuity equation furthermore contains the dimensionless parameter $\gamma =$

175 $\frac{3\tilde{Q}_{s0}}{(1-p)\tilde{U}_0\tilde{Y}_0}$ (with $\tilde{Q}_{s0}$ the sediment transport rate under normal flow conditions and p the

176 bed porosity) and the angle δ which measures deviation of sediment transport from the

177 longitudinal direction. According to *Federici and Seminara* [2003], we may write

$$178 \quad \cos(\delta) = \frac{U}{\|\mathbf{V}\|} \tag{10}$$

$$179 \quad \sin(\delta) = \frac{V}{\|\mathbf{V}\|} - \frac{r}{\beta\sqrt{\tau_\star}}\frac{\partial\eta}{\partial n}. \tag{11}$$

where r is an empirical parameter between 0.5 and 0.6 (see *Colombini et al.* [1987] or *Talmon et al.* [1995]) and $\tau_\star = b\tilde{U}_0^2 U^2$ is the dimensionless Shields stress ($b = \frac{1}{\chi_b^2 d_{50} \frac{\rho_s - \rho_w}{\rho_w}}$, median grain diameter d_{50}, sediment density ρ_s and water density ρ_w). The first term in the right hand side of equations (10) and (11) accounts for the effect of fluid shear stress on particle motion and the second term in equation (11) incorporates gravitational effects of a weak lateral slope (see *Talmon et al.* [1995]). Note that this approximation is only valid in the limit of weak transverse slopes where the effect of gravity is small compared to sediment entrainment by flow. Finally, the dimensionless coefficients of the vegetation equation are related to dimensional variables by the relations $\nu_g = \frac{\alpha_g \tilde{\phi}_m \tilde{Y}_0}{\tilde{U}_0}$, $\nu_D = \frac{D}{\tilde{Y}_0 \tilde{U}_0}$ and $\nu_d = \alpha_d \tilde{Y}_0^2 \tilde{U}_0$.

2.3. Linear stability analysis

We perform a linear stability analysis [*Turing*, 1952] to assess the stability of the 2D-morphodynamic equations coupled with vegetation dynamics (henceforth named ecomorphodynamic equations) around the homogeneous solution $\{U_0, V_0, Y_0, \eta_0, \phi_0\}$, namely a straight river with uniform vegetation density whose dynamics is governed by normal flow conditions. We can then write $\{U_0, V_0, Y_0, \eta_0, \phi_0\} = \{1, 0, 1, -J_0 s, \phi_0\}$ with equilibrium streamwise slope under normal flow conditions J_0 and equilibrium vegetation density ϕ_0 as

$$J_0 = \beta F_0^2 [c_b + c_v \phi_0] \tag{12}$$

$$\phi_{0,1} = \frac{\nu_g - \nu_d}{\nu_g}. \tag{13}$$

Note that there also exists a trivial solution $\phi_{0,2} = 0$ for vegetation density which is inherently unstable for positive $\phi_{0,1}$. Theoretically, $\phi_{0,1}$ may take negative values, but such

solutions are not physically valid since vegetation density can not be negative. In this case, the trivial solution $\phi_{0,2} = 0$ becomes stable and is the only physical solution, meaning that vegetation dynamics is switched off and the model represents a river without riverbed vegetation. Therefore, in order to include vegetation dynamics, parameters have to be chosen in a way to assure a strictly positive solution for $\phi_{0,1}$. In the following, we will use the notation ϕ_0 for $\phi_{0,1}$ assuming a strictly positive uniform solution. Additionally, ϕ_0 needs to be well above zero, meaning that the initial vegetation cover is well-developed, in order to not reach negative values once it is perturbed. Note that the same assumption of well-developed vegetation cover is needed for using a constant-flow description in the presence of a non-constant hydrograph (Section 2.1). We then write the perturbed homogeneous solution as

$$\{1, 0, 1, -J_0 s, \phi_0\} + \epsilon\{U_1, V_1, Y_1, \eta_1, \phi_1\} \tag{14}$$

where for a perturbation with harmonic modes we have in the most general case

$$\begin{pmatrix} U_1 \\ V_1 \\ Y_1 \\ \eta_1 \\ \phi_1 \end{pmatrix} = \begin{pmatrix} u(t)\cos(k_n n + \psi_u) \\ v(t)\cos(k_n n + \psi_v) \\ y(t)\cos(k_n n + \psi_y) \\ h(t)\cos(k_n n + \psi_h) \\ f(t)\cos(k_n n + \psi_f) \end{pmatrix} \exp(ik_s s) + \text{c.c.}. \tag{15}$$

Here, k_n and k_s are the wavenumbers of the harmonic modes in the transverse and streamwise direction while ψ_i are the phases in the transverse direction for each variable. We can further specify the perturbation term by implementing the boundary conditions for impermeable lateral boundaries $V(\pm 1) = 0$ which leads to $k_n = m\frac{\pi}{2}$ with m a positive integer. Note that it can easily be seen that the case where $m = 0$ corresponds to $k_n = 0$ which means that no lateral patterns occur and the model thus reduces to 1D. Figure 5 shows bed elevation patterns for different values of m. While the transverse wavenumber

k_n needs to take discrete values such that the physical transverse half-wavelength $\frac{\tilde{\lambda}_n}{2}$ is a multiple of the actual river width $2\tilde{B}$, no such constraint exists in the streamwise direction. However, note that in principle the longitudinal wavelength corresponding to k_s should be large compared to the normal water depth in order to support the use of the shallow water approximation.

Due to the impermeable lateral boundary, the phase ψ_v in equation (15) can only take the values of 0 and $\frac{\pi}{2}$ which leads us to distinguish the two cases

$$V_1 = v(t)\sin(m\frac{\pi}{2}n)\exp(ik_s s) \qquad (m \text{ odd}) \tag{16}$$

$$V_1 = v(t)\cos(m\frac{\pi}{2}n)\exp(ik_s s) \qquad (m \text{ even}). \tag{17}$$

Finally, in order to have a perturbation Ansatz that is technically convenient, we need the perturbations of the other state variables to be $\frac{\pi}{2}$ out of phase with respect to the perturbation of the transverse velocity V_1 (see for example *Colombini et al.* [1987]) and we get

$$\{U_1, V_1, Y_1, \eta_1, \phi_1\} = \left\{u(t), v(t)\tan^{-1}(m\frac{\pi}{2}n), y(t), h(t), f(t)\right\}\sin(m\frac{\pi}{2}n)\exp(ik_s s) \tag{18}$$

$$\{U_1, V_1, Y_1, \eta_1, \phi_1\} = \left\{u(t), v(t)\tan(m\frac{\pi}{2}n), y(t), h(t), f(t)\right\}\cos(m\frac{\pi}{2}n)\exp(ik_s s) \tag{19}$$

for m odd and even respectively. By this mean, we transform our ecomorphodynamic equation system into an eigenvalue problem with the real parts of the eigenvalues determining the asymptotic fate of the system. Substituting (14), (18) and (19) into equations (3) to (7) we end up with the following linear system of equations:

$$\begin{pmatrix} \frac{du}{dt} \\ \frac{dv}{dt} \\ \frac{dy}{dt} \\ \frac{dh}{dt} \\ \frac{df}{dt} \end{pmatrix} = A \begin{pmatrix} u \\ v \\ y \\ h \\ f \end{pmatrix}, \tag{20}$$

where A is the following 5 x 5 matrix:

$$
\begin{pmatrix}
-ik_s - 2\beta c_b - 2\beta c_v \phi_0 & 0 & \frac{-ik_s}{F_0^2} + \beta c_b & \frac{-ik_s}{F_0^2} & -\beta c_v \\
0 & -ik_s - \beta c_b - \beta c_v \phi_0 & \frac{-k_n(-1)^{m+1}}{F_0^2} & \frac{-k_n(-1)^{m+1}}{F_0^2} & 0 \\
-ik_s & k_n(-1)^{m+1} & -ik_s & 0 & 0 \\
-i\gamma k_s & \frac{1}{3}\gamma k_n(-1)^{m+1} & 0 & -\frac{\gamma r}{3\beta\sqrt{b\tilde{U}_0^2}}k_n^2 & 0 \\
-2\beta\nu_d\phi_0 & 0 & -\beta\nu_d\phi_0 & 0 & -\beta\nu_g\phi_0 - \frac{\nu_{D_s}}{\beta}k_s^2 + \frac{\nu_{D_n}}{\beta}k_n^2
\end{pmatrix}.
$$

$$(21)$$

Equation (20) defines a system of ordinary, homogeneous differential equations with constant coefficients which describes the initial, linear temporal evolution of the perturbed system. In order to assess stability in the limit of long time t in the linear regime, the real parts of the eigenvalues ω_i of matrix A may be analyzed [*Camporeale and Ridolfi*, 2009]. We can say that the system is stable with respect to a perturbation with longitudinal wavenumber k_s and bar order m if $\text{Max}_i(\text{Re}(\omega_i(k_s, m))) < 0$, meaning that all perturbations decay in time. Conversely, the system is unstable if for any given perturbation we have $\text{Max}_i(\text{Re}(\omega(k_s, m))) > 0$. More importantly, the system is unstable towards periodic spatial patterns in the linear regime if the highest growth rate $\text{Max}_i(\text{Re}(\omega_i(k_s, m)))$ occurs at finite streamwise wavenumber k_s with all parameters fixed. In this case, for fixed k_s, perturbation growth rate as a function of bar order m determines whether the system evolves towards alternate ($m = 1$) or multiple bars ($m > 1$).

3. Results

3.1. 1-dimensional analysis

We start our analysis with the case of a relatively narrow river where we can safely use a 1D model. The unstable waves that can develop in such rivers are referred to as long waves (see also the analysis of *Lanzoni et al.* [2006]). In principle, the 1D equations can be obtained as a special case from equation (20) by setting $m = 0$. However, the conventions found in the literature differ when considering 1D ([*Lanzoni et al.*, 2006]) or 2D setups [*Federici and Seminara*, 2003] due to different choices of dimensionless quantities. In order to be able to compare our results to the existing literature, we therefore need to rewrite the model in the following one-dimensional form:

$$\frac{\partial U}{\partial t} = -U\frac{\partial U}{\partial s} - \frac{1}{F_0^2}\left[\frac{\partial Y}{\partial s} + \frac{\partial \eta}{\partial s}\right] - c_b\frac{U^2}{Y} - c_v\phi U^2 \tag{22}$$

$$\frac{\partial Y}{\partial t} = -Y\frac{\partial U}{\partial s} - U\frac{\partial Y}{\partial s} \tag{23}$$

$$\frac{\partial \eta}{\partial t} = -\gamma U^2\frac{\partial U}{\partial s} \tag{24}$$

$$\frac{\partial \phi}{\partial t} = \nu_g\phi(1-\phi) + \nu_D\frac{\partial^2\phi}{\partial s^2} - \nu_d\phi Y U^2, \tag{25}$$

where $F_0 = \frac{\tilde{U}_0}{\sqrt{g\tilde{Y}_0}}$, $c_b = \frac{g}{\chi_b^2}$, $c_v = \frac{c_D d\tilde{\phi}_m\tilde{Y}_0}{2}$, $\gamma = \frac{3\tilde{Q}_{s0}}{(1-p)\tilde{U}_0\tilde{Y}_0}$, $\nu_g = \frac{\alpha_g\tilde{\phi}_m\tilde{Y}_0}{\tilde{U}_0}$, $\nu_D = \frac{D}{\tilde{Y}_0\tilde{U}_0}$ and $\nu_d = \alpha_d\tilde{Y}_0^2\tilde{U}_0$. Note that the streamwise coordinate and time are normalized as $s = \tilde{Y}^{-1}\tilde{s}$ and $t = \tilde{U}_0\tilde{Y}^{-1}\tilde{t}$, while $U = \tilde{U}_0^{-1}\tilde{U}$, $\{Y,\eta\} = \tilde{Y}_0^{-1}\{\tilde{Y},\tilde{\eta}\}$ and $\phi = \tilde{\phi}_m^{-1}\tilde{\phi}$ remain unchanged with respect to the 2D model.

It is well known [*Lanzoni et al.*, 2006] that in the linear regime of the morphodynamic equations no instability can be detected at finite wavenumber. Instability at the linear regime can only be found for a fixed bed and $F_0 > 2$ but then the selected wavenumber is $k_s = \infty$ (roll waves, see *Lanzoni et al.* [2006]). This means that the system of equations (22), (23) and (24) with $\tilde{\phi}_m$ alone can not produce instability towards periodic patterns at

278   the linear level. Note that in the long term nonlinear effect could still trigger instabilities

279   that lead to patterns.

280   We will now see what happens if we first combine vegetation dynamics with flow dynamics

281   while assuming fixed bed conditions (equations (22), (23) and (25), putting equal to zero

282   the sediment parameter γ). While vegetation growing on a fixed bed may seem unrealistic

283   it provides a useful insight into the fundamental effects of flow-vegetation interaction.

284   In Figure 6A, B and C, different vegetation coefficients are varied and plotted along with

285   Froude number F_0 at fixed water depth. It is clearly visible on all three figures that

286   the dynamic interaction between flow and vegetation causes instability towards periodic

287   patterns in certain regions of the parameter space. Furthermore, the domain proves to be

288   simply connected, meaning that it does not possess any holes. Note that in Figures 6A and

289   B the domain extends down to the origin. Additionally, the pattern wavenumber increases

290   with increasing Froude number, carrying capacity and growth rate. Those findings remain

291   valid if sediment dynamics is added to the equation system by allowing $\gamma > 0$: we can see

292   in figure 6D that γ only becomes relevant at values greater than 10^{-1}. But, due to the fact

293   that γ represents the ratio of the sediment timescale to the hydrodynamic timescale its

294   actual value is generally much lower ($\gamma \sim \mathcal{O}(10^{-3} - 10^{-4})$, see *Parker* [1976] for realistic

295   estimates).

3.2. 2-dimensional analysis

296   Having seen in the previous section that our simple vegetation model indeed can lead

297   to periodic patterns, we now focus on the 2D model which is more relevant for natural

298   rivers. In view of readability, we will use the abbreviations SV for Saint-Venant, SVE

299   for Saint-Venant-Exner, SVV for Saint-Venant-Vegetation and SVEV for Saint-Venant-

300 Exner-Vegetation (see also Table 1).

301 As shown by *Colombini et al.* [1987], flow-sediment instability can be found above a cer-

302 tain threshold for the aspect ratio β (Figure 2) if an appropriate model for transverse

303 slope effects on sediment transport is chosen (equation (11)). In Figure 7A, we reproduce

304 the classical result from *Colombini et al.* [1987] using our 2D model without the vegetation

305 equation. The color code indicates the maximum growth rate and the black line shows

306 the selected longitudinal wavenumber k_s for a certain aspect ratio β. Then, in Figure 8A

307 we can see pattern domains of alternate and multiple bars in the F_0 vs. β space based

308 on comparing the growth rates for different values of the bar order m. Note that higher

309 aspect ratio and Froude number correspond to higher bar order m of the most unstable

310 perturbation. Additionally, a sharp cut-off is visible at about $F_0 = 2$, meaning that no

311 instability towards finite patterns occurs if $F_0 > 2$ independent of the aspect ratio. This

312 is because above the critical value $F_0 = 2$ modes with unbounded wavenumber experience

313 a higher growth rate than patterns with finite wavenumber (analogous to the roll waves

314 in the 1D model).

315 While the graphs in Figures 7A and 8A represent a river with movable bed but devoid of

316 vegetation, 7B and 8B are their equivalents for a vegetated river with fixed bed (i.e. no

317 erosion). The qualitative similarity between Figures 7A and B is striking (note however

318 the difference in the value of the Froude number): the pattern domain is "U-shaped" and

319 there is an aspect ratio threshold for observing patterns. This means that for certain

320 parameter values the vegetation equation (coupled with flow) produces instability at a

321 finite wavelength, which is confirmed by Figure 8B where we can see the characteristic

322 shape of the vegetation-flow instability domain in the Froude number versus aspect ratio

space. We observe a left and a right boundary with a sharp cut-off to the right along

with a minimum value for the aspect ratio. In contrast to Figure 8A, the cut-off is due

to the fact that a river's uprooting capacity is proportional to the Froude number and

thus the stable equilibrium solution of vegetation density ϕ_0 becomes zero above a certain

Froude number (to the right of the black line of Figure 8B). Note that strictly speaking

our assumption of well-developed vegetation cover (ϕ_0 well above zero) is not fullfilled

anymore close to the limiting Froude number where ϕ_0 tends to zero.

Interestingly though, only alternate bar patterns are produced by vegetation growing

on a fixed bed (Figure 8B). This means that the growth rate of alternate bars always

exceeds that of multiple bars (of any order), a fact which holds independently of the

Froude number or aspect ratio. This result is related to the fact that when assuming

a reasonable value for vegetation density its induced roughness always exceeds sediment

induced roughness by at least an order of magnitude.

After discussing vegetation- and sediment-related patterns alone, we tackle now the com-

plete problem with a full coupling between sediment and vegetation dynamics. Thus, in

the following we are showing the results of the complete model developed in Section 2.2

which describes 2-dimensional flow on a movable, vegetated river bed. Figure 9 shows

comparisons of SVV and SVEV (alternate bar formation only) in the F_0 vs. vegetation

carrying capacity $\tilde{\phi}_m$ and F_0 vs. β space respectively. Figure 9A indicates that the same

competitive interaction between vegetation growth and death is taking place as was seen

for the 1D model. It then turns out that the inclusion of sediment dynamics does (for a

realistic range of values for γ, see Section 3.1) not deform an existing instability domain

but rather add to it. We can therefore conclude on the influence of sediment dynam-

346 ics by simply looking at what is added in the graphs below with respect to the graphs

347 above in Figure 9. As expected, to the right of the black line where no vegetation occurs

348 we retrieve the instability domain induced by sediment dynamics alone with a cut-off at

349 $F_0 = 2$. Additionally, we can see another instability domain at lower Froude number

350 in Figure 9C which seems to be the result of the interplay of sediment and vegetation

351 dynamics. While vegetation adds instability domains we can also see that part of the

352 pattern domain previously present in the SVE-model (Figure 8A) disappeared. Further-

353 more, Figure 9D indicates that, different to the domains resulting from the 1D analysis,

354 the pattern domain is no more simply connected. In fact, the domain is divided in two

355 parts in the F_0 vs. β space with part of the sediment-induced instability detached from

356 the main domain. Incidentally, this is also visible in Figure 9C for the horizontal line

357 $\tilde{\phi}_m = 10$.

358 The dominating longitudinal wavenumber k_s depends heavily on the model parameters and

359 can also vary drastically in the same graph. For example in Figure 9D, lower wavenumbers

360 (and thus higher wavelengths) occur on the higher-Froude number half of the vegetation

361 domain and on the part of the sediment domain that is attached to the vegetation domain

362 while higher wavenumbers can be seen on the lower-Froude number half of the vegetation

363 domain and for small Froude numbers.

364 Figure 10 shows from another viewpoint which part of the instability domain is caused by

365 sediment dynamics and vegetation dynamics respectively. In fact, the two graphs are ver-

366 tical profiles of Figure 9D, the upper one for $F_0 = 0.65$ showing contribution of sediment

367 dynamics (note the similarity to Figure 7A) while the lower one for $F_0 = 0.75$ contains the

368 influence of both sediment (aspect ratio below 30) and vegetation (aspect ratio above 30,

see also 7B. We can thus observe that the left part of the instability domain (with lower

longitudinal wavenumbers) to the right in Figure 9D is caused by sediment dynamics.

In contrast, the dark blue part (having higher longitudinal wavenumbers) of the same

instability domain is clearly due to vegetation dynamics, as it can be seen in Figure 10B.

As we already saw the pattern domains for formation of alternate bars in the model

including sediment and vegetation dynamics, we finally want to turn our attention to

the formation of multiple bars. For this aim, we again compare the results of the model

without sediment dynamics (SVV) to the full model (SVEV). Essentially, Figure 11 cor-

responds to the right side of Figure 9 but with a color code indicating bar order instead

of selected longitudinal wavenumber. Again, we can observe how the pattern domains

of sediment dynamics (Figure 7B) and vegetation are merged to yield a different kind

of domain. Note the abrupt change from multiple bar formation with increasing aspect

ratio to only alternate bar formation in the vegetation-induced domain to multiple bar

formation again (left to right). While only part of the sediment-induced instability to-

wards multiple bars is preserved (but interrupted in the middle), the vegetation-induced

part is completely preserved and still leads to alternate bars exclusively. It can be seen

in Figure 12 (A and B are both normalized with respect to the highest growth rate in

A) that the vegetation-induced instability domain of alternate bars (m=1) contains the

domain of multiple bars (m=4) and that its growth rate is always higher. This is true for

multiple bars of any order.

4. Discussion

We showed that by using stability analysis of our ecomorphodynamic framework we indeed can detect instability towards periodic patterns with finite wavelength. The essential ingredient for such instability to occur in the 1D model is competitive interaction between vegetation growth and mortality caused by flow drag. In this context, competitive interaction means that there is at least one mechanism (i.e., biomass growth in our case) that increases vegetation density ϕ and another one (i.e., uprooting by flow drag in our mode) that counteracts it (*D'Odorico et al.* [2007] and *Crouzy et al.* [2015]). This competitive interaction creates opportunities for the presence of patterns meaning that vegetation is neither present everywhere nor completely missing. In our model uprooting depends on water depth and velocity. Hence, the balance between such state variables is dynamic, thus favoring growth of vegetation in some cases and death in others. Eventually, this may result in vegetation patterns that are either in phase or out-of-phase with hydrodynamic variables.

While it is well known that the 1D morphodynamic framework without vegetation (SVE) does not exhibit instability towards regular patterns, it was unknown how sediment dynamics can influence vegetation induced river patterns. We found that in the presence of significant vegetation density sediment dynamics does not contribute actively to pattern formation, due to vegetation induced roughness dominating sediment induced roughness. Instead bed topography adapts in a passive manner to vegetation induced patterns. It is interesting that this was found to be true independent of the values assigned to the vegetation coefficients. After fixing the less fundamental parameters (Table 3), we identified four parameters (three describing vegetation and one describing flow) mostly relevant for

₄₁₂ such competitive interaction: the growth rate α_g and the carrying capacity $\tilde{\phi}_m$ promote

₄₁₃ growth while the mortality rate α_d and the Froude number F_0 (at constant water depth)

₄₁₄ lead to a higher mortality through uprooting.

₄₁₅ In contrast to the 1D SVE morphodynamic framework, its extension to two dimensions

₄₁₆ was shown to allow for regular patterns once a certain threshold for the aspect ratio

₄₁₇ is exceeded (*Colombini et al.* [1987] and *Federici and Seminara* [2003]). Moreover, this

₄₁₈ threshold seemed to match reasonably well the available empirical data [*Colombini et al.*,

₄₁₉ 1987]. An important ingredient of the morphodynamic models of *Colombini et al.* [1987]

₄₂₀ and *Federici and Seminara* [2003] is a semi-empirical relationship for lateral slope effects

₄₂₁ in rivers (see *Talmon et al.* [1995] for the derivation). This relationship expresses the fact

₄₂₂ that sediment transport is not following bottom shear stress exactly in the presence of a

₄₂₃ laterally sloped bed, but is slightly deviated due to gravitaional forces along the lateral

₄₂₄ slope. Although the previous works did not insist on this, the correction for sediment

₄₂₅ transport seems to be an essential element for reproducing the well-known threshold of

₄₂₆ the aspect ratio below which no instability towards patterns occurs.

₄₂₇ In this work, we extended the well-known 2D SVE morphodynamic framework to account

₄₂₈ for riverbed vegetation and we found the same competitive interaction between vegetation

₄₂₉ growth and death as in the 1D model to be responsible for instability towards patterns

₄₃₀ on a fixed river bed with vegetation. Vegetation density increases local roughness and

₄₃₁ locally slows the stream velocity with consequent increase of water depth. In our model,

₄₃₂ this mechanisms favors sediment deposition and bed aggradation, and has thus an in-

₄₃₃ direct effect on vegetation growth. Although in reality these morphogenic mechanisms

₄₃₄ are conjectured to drive vegetation growth, we found that the emergence of vegetated

patterns can be either in phase or not with hydromorphodynamic variables depending on how the latter combine to determine uprooting. Remarkably, this vegetation-induced pattern domain also exhibits a lower threshold for the aspect ratio but the domain generally occurs at higher longitudinal wavenumber k_s than sediment-induced domains. It thus seems that both kinds of patterns, vegetation-induced and sediment-induced ones, need a certain minimum lateral length-scale in order to develop and are not freely scalable. The analysis of the complete 2D framework showed that although the instability towards multiple bars needs a movable bed to be triggered, the vegetation parameters still affect the Froude number at which this instability occurs. Thus, even if it is neither a necessary nor a sufficient condition for pattern formation, riverbed vegetation has to be taken into account in order to know under which conditions such patterns prevail and to determine the dominant longitudinal wavelength.

Comparing our work to numerical models for the effect of vegetation on river patterns (e.g. *Murray and Paola* [2003] and *Crosato and Saleh* [2011]), we can see an interesting agreement to our results. In fact, these studies suggest that a river will typically develop a braiding pattern in an unvegetated floodplain while the tendency to meander increases with increasing vegetation density. Similarly, using our analytical framework we found multiple bars (braiding) to prevail on unvegetated floodplains. Conversely, the addition of vegetation dynamics clearly produced a region in the parameter domain where only instability towards alternate bars exists, which can be considered the first step in the development of meanders [*Ikeda et al.*, 1981]. The coincidence of these results is particularly interesting considering the fact that *Murray and Paola* [2003] and *Crosato and Saleh*

458 [2011] include riverbed vegetation by means of increased bank strength while in this work

459 we focus on vegetation-induced roughness change.

460 Our modeling approach, including a minimal model for vegetation dynamics, allows the

461 use of a systematic stability analysis to detect parameter domains with periodic river

462 patterns. However, it leads to the omission of a number of potentially important pro-

463 cesses. Some of them could be readily added to the present model in a next step. For

464 instance, flow diversion caused by riverbed vegetation could be taken into account by

465 adding an appropriate term in the flow-continuity equation (equation (5)). It was not

466 taken into account in this analysis since vegetation volume is negligibly small compared

467 to water volume in our model setup. In fact, the volume percentage occupied by vegeta-

468 tion is around 0.1 percent while vegetation induced roughness is ten times larger than bed

469 roughness for typical parameters. Furthermore, we could extend our work to submerged

470 or flexible vegetation (as opposed to the non-submerged, rigid vegetation we assumed in

471 this analysis). For completely submerged vegetation the surface impacted by flow drag

472 would be reduced by a factor of $\frac{\tilde{h}_v}{\tilde{Y}}$ (with $\tilde{h}_v$ the vegetation height) in the third term on

473 the right hand side of equation (7). Meanwhile, non-rigid vegetation would require the

474 exponent of $\tilde{U}$ to be somewhere between 1 and 2 in the same term.

475 None of the above-mentioned processes however is expected to significantly alter the gen-

476 eral results of this work as long as a flow regime allowing a competition between growth

477 and death is observed. However, the shape of the instability domains in the parameter

478 space could be modified. In contrast, the vegetation cover would either colonize the whole

479 riverbed if the floods were too low or too short or get completely destroyed if the floods

480 were too strong or too long and thus vegetation-induced patterns would not exist any-

more.

Perhaps the two major effects related to riverbed vegetation that were not considered in this analysis are related to roots. Firstly, the presence of roots is known to increase bed stability [*Pasquale and Perona*, 2014]. Secondly, the erosion of sediment around a plant can expose the root system which makes the plant more susceptible to uprooting due to reduced root anchoring (Type II mechanism in *Edmaier et al.* [2011]). Additionally, uprooting is not an instantaneous process anymore but a more gradual one where several floodings can contribute to root exposure until uprooting finally takes place [*Edmaier et al.*, 2015]. The inclusion of the first of the two aforementioned effects would require the introduction of an additional term on the right hand side of equation (6). This term would include a threshold related to root strength and sediment transport would only start once this threshold is exceeded. Integrating the second effect would require the proportionality constant ν_d in equation (7) to be a function of plant rooting depth and bed elevation in order to determine the amount of roots exposed at a given time. As opposed to the modifications mentioned earlier, the latter two are fundamentally different processes which could potentially alter the pattern forming dynamics. Nevertheless, they introduce significant technical complications and are thus not well suited for an analytically tractable model. Another possibility consists of modeling vegetation mortality as a function of bed elevation change ($\frac{\partial \eta}{\partial t}$. Positive values of $\frac{\partial \eta}{\partial t}$ would mean vegetation burying while negative values represent roots exposure, both eventually leading to the death of vegetation.

While further terms can readily be added to our ecomorphodynamic equations without implying essential conceptual or technical changes, the assumption of a uniformly-vegetated state perturbed by flooding events appears to be an intrinsic limitation of our frame-

504 work. Linear perturbation analysis performed over a state with regions without vegetation

505 would indeed directly lead to non-physical solutions with negative vegetation density. This

506 threshold at zero density introduces in turn a non-linearity probably precluding an ana-

507 lytical treatment. In this regard, numerical simulations of our ecomorphodynamic model

508 could shed light on whether the non-linearity yields fundamentally different results. In

509 rivers, our model is thus fully appropriate to describe regions subject to intermittent flow,

510 as riverbars where a homogenous cover of pioneer vegetation may develop before the onset

511 of flooding events, or the inner of meander bends where vegetated stripes are observed

512 (so-called scroll bars). The importance of flow intermittency lead us to the generaliza-

513 tion of the ecomorphodynamic model integrating flooding and drought periods. Leaving

514 classical rivers, tidal marshes could offer an example of vegetation growing while subject

515 to action of the flow. Note that in order to apply our framework to this case one should

516 consider flexible vegetation instead of rigid vegetation.

517 In this work, we analyzed the behavior of our ecomorphodynamic model in the asymptotic

518 limit in the linear regime and thus all conclusions are restricted to this limit, meaning

519 that nonlinear effects need to be weak. If the operator A in equation possesses N distinct

520 eigenvalues (where N is the rank of A) as it is in the present problem we can write the

521 general solution of (20) as

$$\sum_{i=1}^{N} c_i \exp(\omega_i t)\mathbf{v}_i, \tag{26}$$

523 where ω_i are the complex eigenvalues of A, $\mathbf{v}_i$ are the respective eigenvectors and c_i are

524 coefficients. If A were a normal operator (meaning that $AA^* = A^*A$), we could find an

525 orthogonal basis of eigenvectors $\mathbf{v}_i$. In the limit of large t then, the system would be

526 dominated by the exponential with the largest temporal growth rate (maximum of the

real parts of ω_i) and thus the solution would decay to zero for a negative maximum growth rate and grow for a positive maximum growth rate. Note that this is only true in the linear regime and that nonlinear effects could come into play at some point.

However, in the context of river morphology, A is not a normal operator and therefore its eigenvectors do not form an orthogonal basis. That is, although the system may be asymptotically stable, transient growth can still occur [*Camporeale and Ridolfi*, 2009] at finite timescales. Therefore, further research needs to be done if the timescale of interest is finite [*Camporeale and Ridolfi*, 2009]. But, asymptotically the exponential with the largest real part of the eigenvalues is still going to dominate and thus describes the behavior of the system as t becomes large. This is why we can still safely state that the initially small perturbations will be amplified in the long-term linear regime if the real part of any ω_i is positive. And if the largest growth rate occurs for a finite longitudinal wavenumber k_s (all parameters fixed), this mode will be amplified more strongly than all other modes contained in a packet of random perturbation waves and thus will dominate after some time due to the exponential character of perturbation growth.

Finally, since our model is designed to include only the main effects of riverbed vegetation on river morphology, one could think of using field data to evaluate the accuracy of these design choices in a realistic scenario (e.g., see Figure 1). However, although ecomorphodynamics is a field which has rapidly been expanding over the last few years, we were not able to find out a field dataset allowing a comprehensive validation of the results of our stability analysis (or equivalently also allowing to falsify our theory). Regarding field studies, one can cite the difficulty of identifying a typical dominant flow essential for a quantitative comparison with the theory. Flume experiments allow a better control of

the flow and sediment conditions, however, identifying the perfect lab model for riparian vegetation is still challenging (**?**). It is interesting to note that we have used our ecomorphodynamic model to interpret the results of a flume experiment in a convergent channel (1D setup, *Perona et al.* [2014]). Obtaining comprehensive results on the 2D setup would be challenging but could constitute a very interesting continuation of our study. We hope that our results could help motivating and designing such experiments.

5. Conclusion

In this work, we developed an analytical model for riverbed vegetation dynamics and coupled it to the classic two-dimensional Saint Venant-Exner framework to obtain a set of ecomorphodynamic equations. Subsequently, we performed a linear stability analysis of the ecomorphodynamic equations and assessed its capability to produce periodic river patterns.

We found that competitive interaction between vegetation growth and mortality indeed may lead to instability towards longitudinal waves in a one-dimensional framework with bed elevation following the vegetation pattern. In the two-dimensional framework, alternate bars develop on a fixed bed while both alternate and multiple bars can be found on a movable bed. While it is known [*Engelund and Skovgaard*, 1973] that stability analysis of large, unvegetated rivers predicts instability towards multiple bars which can be seen as a possible precursor of braiding, the addition of vegetation dynamics in our model tends to favor meandering instead. Remarkably, this is compatible with the findings of numerical simulations which include the bank-strengthening effect of riparian vegetation, although in our work vegetation acts on roughness instead of bank strength.

References

Baptist, M., V. Babovic, J. Rodríguez Uthurburu, M. Keijzer, R. Uittenbogaard, A. Mynett, and A. Verwey (2007), On inducing equations for vegetation resistance, *Journal of Hydraulic Research*, *45*(4), 435–450.

Bertoldi, W., A. Siviglia, S. Tettamanti, M. Toffolon, D. Vetsch, and S. Francalanci (2014), Modeling vegetation controls on fluvial morphological trajectories, *Geophysical Research Letters*, *41*(20), 7167–7175.

Blondeaux, P., and G. Seminara (1985), A unified bar–bend theory of river meanders, *Journal of Fluid Mechanics*, *157*, 449–470.

Callander, R. (1969), Instability and river channels, *Journal of Fluid Mechanics*, *36*(03), 465–480.

Camporeale, C., and L. Ridolfi (2006), Riparian vegetation distribution induced by river flow variability: A stochastic approach, *Water Resources Research*, *42*(10).

Camporeale, C., and L. Ridolfi (2009), Nonnormality and transient behavior of the de Saint-Venant-Exner equations, *Water resources research*, *45*(8).

Camporeale, C., E. Perucca, L. Ridolfi, and A. Gurnell (2013), Modeling the interactions between river morphodynamics and riparian vegetation, *Reviews of Geophysics*, *51*(3), 379–414.

Colombini, M., G. Seminara, and M. Tubino (1987), Finite-amplitude alternate bars, *Journal of Fluid Mechanics*, *181*, 213–232.

Coulthard, T. J. (2005), Effects of vegetation on braided stream pattern and dynamics, *Water Resources Research*, *41*(4).

Crosato, A., and M. S. Saleh (2011), Numerical study on the effects of floodplain vegetation on river planform style, *Earth Surface Processes and Landforms*, *36*(6), 711–720.

Crouzy, B., F. Bärenbold, P. DOdorico, and P. Perona (2015), Ecomorphodynamic approaches to river anabranching patterns, *Advances in Water Resources*.

Davies, N. S., and M. R. Gibling (2010), Cambrian to Devonian evolution of alluvial systems: the sedimentological impact of the earliest land plants, *Earth-Science Reviews*, *98*(3), 171–200.

D'Odorico, P., F. Laio, A. Porporato, L. Ridolfi, and N. Barbier (2007), Noise-induced vegetation patterns in fire-prone savannas, *Journal of Geophysical Research: Biogeosciences (2005–2012)*, *112*(G2).

Edmaier, K., P. Burlando, and P. Perona (2011), Mechanisms of vegetation uprooting by flow in alluvial non-cohesive sediment, *Hydrology and Earth System Sciences Discussions*, *8*(1), 1365–1398, doi:10.5194/hessd-8-1365-2011.

Edmaier, K., B. Crouzy, and P. Perona (2015), Experimental characterization of vegetation uprooting by flow, *Journal of Geophysical Research: Biogeosciences*.

Engelund, F., and O. Skovgaard (1973), On the origin of meandering and braiding in alluvial streams, *Journal of Fluid Mechanics*, *57*(02), 289–302.

Federici, B., and C. Paola (2003), Dynamics of channel bifurcations in noncohesive sediments, *Water Resources Research*, *39*(6).

Federici, B., and G. Seminara (2003), On the convective nature of bar instability, *Journal of Fluid Mechanics*, *487*, 125–145.

Gibling, M. R., and N. S. Davies (2012), Palaeozoic landscapes shaped by plant evolution, *Nature Geoscience*, *5*(2), 99–105.

622 Gurnell, A., and G. Petts (2006), Trees as riparian engineers: the Tagliamento River,

623 Italy, *Earth Surface Processes and Landforms*, *31*(12), 1558–1574.

624 Gurnell, A. M., W. Bertoldi, and D. Corenblit (2012), Changing river channels: The roles

625 of hydrological processes, plants and pioneer fluvial landforms in humid temperate,

626 mixed load, gravel bed rivers, *Earth-Science Reviews*, *111*(1), 129–141.

627 Ikeda, S., G. Parker, and K. Sawai (1981), Bend theory of river meanders. Part 1. Linear

628 development, *Journal of Fluid Mechanics*, *112*, 363–377.

629 Jansen, J. D., and G. C. Nanson (2010), Functional relationships between vegetation,

630 channel morphology, and flow efficiency in an alluvial (anabranching) river, *Journal of*

631 *Geophysical Research: Earth Surface (2003–2012)*, *115*(F4).

632 Lanzoni, S., A. Siviglia, A. Frascati, and G. Seminara (2006), Long waves in erodible

633 channels and morphodynamic influence, *Water resources research*, *42*(6).

634 Li, S., and R. Millar (2011), A two-dimensional morphodynamic model of gravel-bed river

635 with floodplain vegetation, *Earth Surface Processes and Landforms*, *36*(2), 190–202.

636 Murray, A. B., and C. Paola (2003), Modelling the effect of vegetation on channel pattern

637 in bedload rivers, *Earth Surface Processes and Landforms*, *28*(2), 131–143.

638 Nepf, H. M. (2012), Flow and transport in regions with aquatic vegetation, *Annual Review*

639 *of Fluid Mechanics*, *44*, 123–142.

640 Nicholas, A., P. Ashworth, G. Sambrook Smith, and S. Sandbach (2013), Numerical

641 simulation of bar and island morphodynamics in anabranching megarivers, *Journal of*

642 *Geophysical Research: Earth Surface*, *118*(4), 2019–2044.

643 Parker, G. (1976), On the cause and characteristic scales of meandering and braiding in

644 rivers, *Journal of Fluid Mechanics*, *76*(03), 457–480.

Pasquale, N., and P. Perona (2014), Experimental assessment of riverbed sediment rein-
    forcement by vegetation roots, in *River Flow 2014-IAHR-International Conference on
    River Hydraulics*, EPFL-CONF-199441.

Pasquale, N., P. Perona, P. Schneider, J. Shrestha, A. Wombacher, and P. Burlando
    (2010), Modern comprehensive approach to monitor the morphodynamic evolution of
    restored river corridors, *Hydrology and Earth System Sciences Discussions*, *7*(6), 8873–
    8912.

Perona, P., P. Molnar, B. Crouzy, E. Perucca, Z. Jiang, S. McLelland, D. Wüthrich,
    K. Edmaier, R. Francis, C. Camporeale, et al. (2012), Biomass selection by floods and
    related timescales: Part 1. Experimental observations, *Advances in Water Resources*,
    39, 85–96.

Perona, P., B. Crouzy, S. McLelland, P. Molnar, and C. Camporeale (2014), Ecomorpho-
    dynamics of rivers with converging boundaries, *Earth Surface Processes and Landforms*,
    39(12), 1651–1662.

Perucca, E., C. Camporeale, and L. Ridolfi (2007), Significance of the riparian vegetation
    dynamics on meandering river morphodynamics, *Water Resources Research*, *43*(3).

Pollen, N., and A. Simon (2005), Estimating the mechanical effects of riparian vegetation
    on stream bank stability using a fiber bundle model, *Water Resources Research*, *41*(7).

Seminara, G. (2010), Fluvial sedimentary patterns, *Annual Review of Fluid Mechanics*,
    42, 43–66.

Tal, M., and C. Paola (2007), Dynamic single-thread channels maintained by the interac-
   tion of flow and vegetation, *Geology*, *35*(4), 347–350.

Talmon, A., N. Struiksma, and M. Van Mierlo (1995), Laboratory measurements of the direction of sediment transport on transverse alluvial-bed slopes, *Journal of Hydraulic Research*, *33*(4), 495–517.

Tooth, S., and G. C. Nanson (2000), The role of vegetation in the formation of anabranching channels in an ephemeral river, Northern plains, arid central Australia, *Hydrological processes*, *14*(16-17), 3099–3117.

Tooth, S., and G. C. Nanson (2004), Forms and processes of two highly contrasting rivers in arid central Australia, and the implications for channel-pattern discrimination and prediction, *Geological Society of America Bulletin*, *116*(7-8), 802–816.

Turing, A. M. (1952), The Chemical Basis of Morphogenesis, *Philosophical Transactions of the Royal Society of London. Series B, Biological Sciences*, *237*(641), 37–72, doi: 10.1098/rstb.1952.0012.
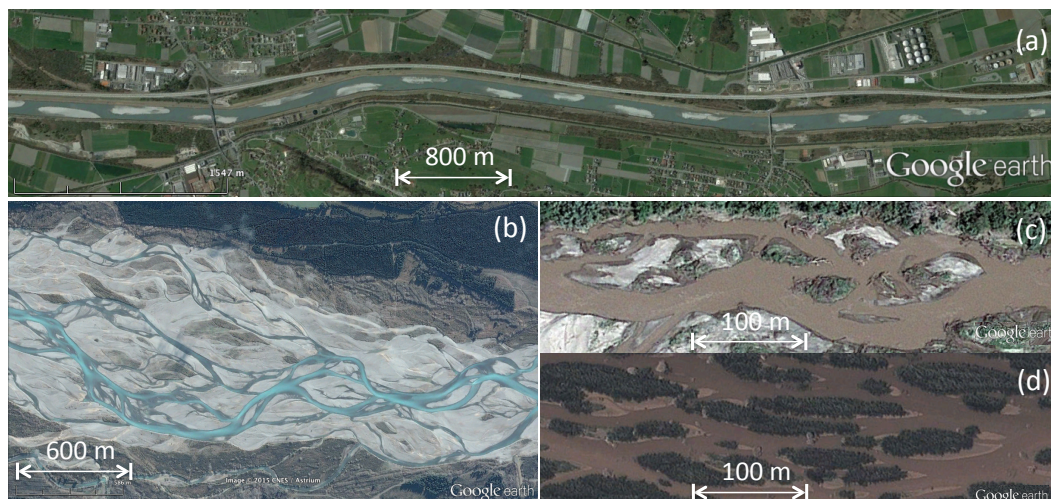
Figure 1.   Examples of river bed patterns emerging in different environments: A) regular series of unvegetated alternate bars on the Rhine River (Haag, Switzerland; B) braided river in absence of vegetation (Waimakariri River, New Zealand); C) moderately vegetated multiple bars (Awash River, Ethiopia); D) anabranching patterns in the form of completely vegetated multiple bars (Awash River, Ethiopia). Map data: Google, Digitalglobe.
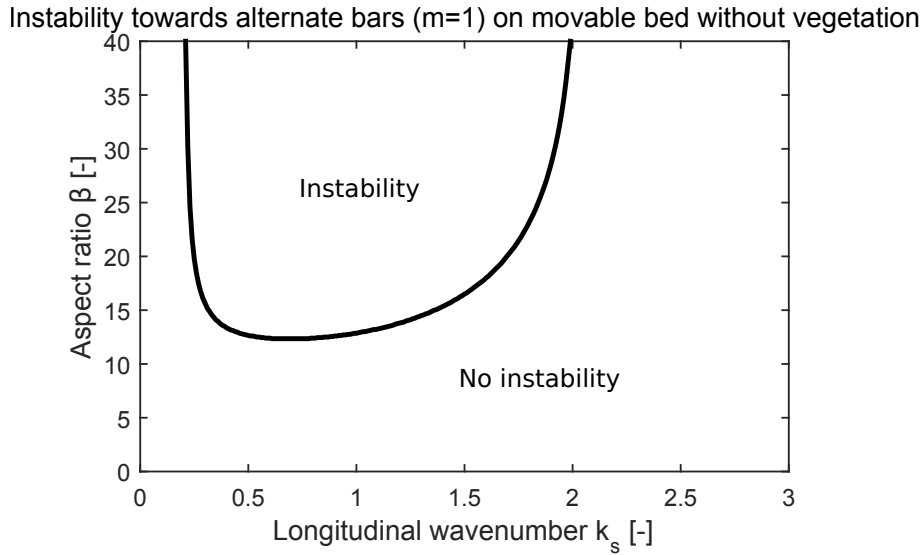
Figure 2. Neutral curve for alternate bar formation (instability towards alternate bars above the line, no instability below) in the k_s vs. β space.
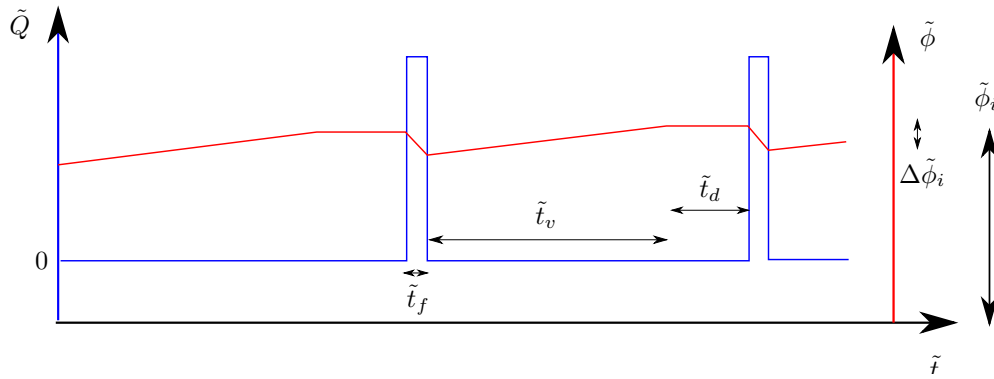
Figure 3. Idealized river hydrograph with non-constant flow: the blue curve represents water discharge ($\tilde{Q}$); the red curve represents vegetation density ($\tilde{\phi}$). $\tilde{\phi}_i$ the vegetation density after cycle i and $\Delta\tilde{\phi}_i$ the change of vegetation density during cycle i. Flooding timescale t_f, vegetation timescale t_v and drought timescale t_d are indicated in black.
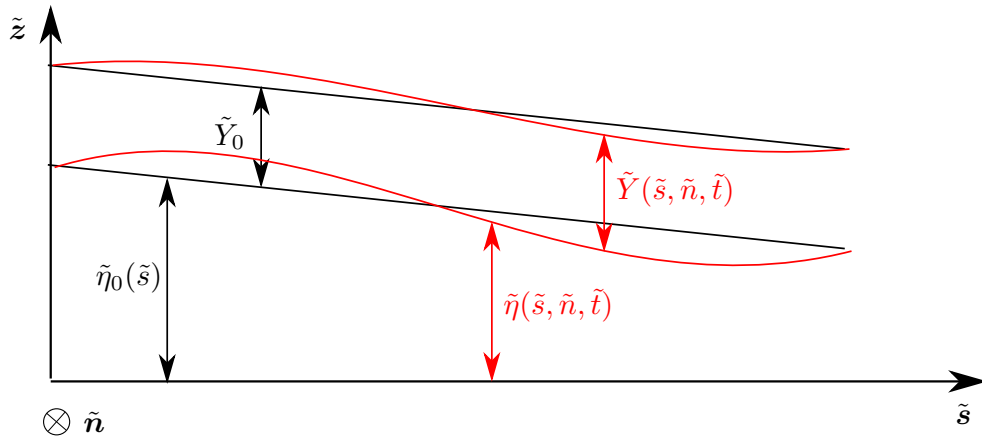
Figure 4.   Uniform water height $\tilde{Y}_0$ and bed profile $\tilde{\eta}_0(\tilde{s})$ in black and perturbed water height $Y_0(\tilde{s}, \tilde{n}, \tilde{t})$ and bed profile $\tilde{\eta}(\tilde{s}, \tilde{n}, \tilde{t})$ in red.
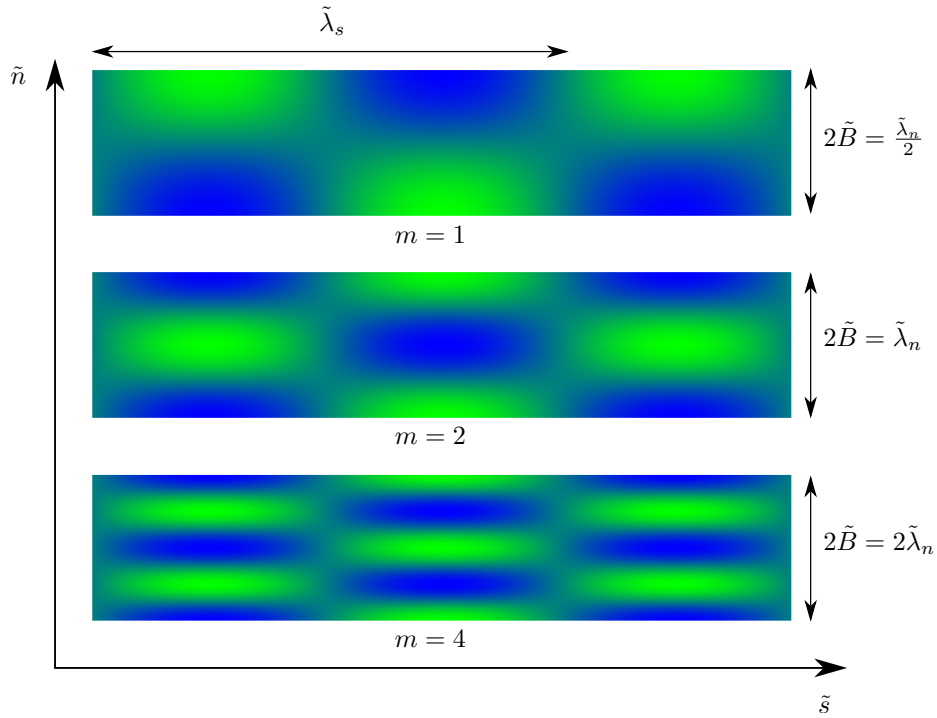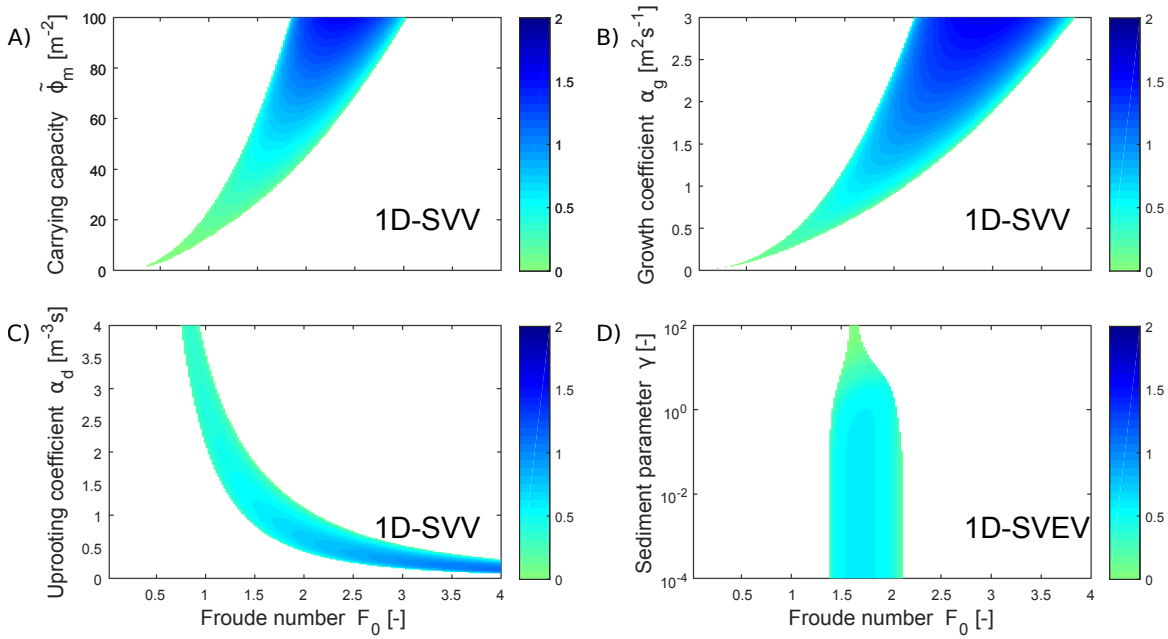

Figure 5.   Top view of bed elevation for alternate ($m = 1$) and multiple bars ($m > 1$), blue indicates lower elevation.

Table 2. Fixed parameters of the 1D analysis

| Parameter name	Variable	Value	Units
Normal water depth	$\tilde{Y}_0$	1	m
Stokes drag coefficient	c_D	1.5	-
Vegetation diameter	d	0.01	m
Strickler coefficient	k_{st}	33.33	$m^{1/3}s^{-1}$
Vegetation diffusion coefficient	D	0	m^2s^{-1}

Figure 6. 1D instability domains of SVV and SVEV: white means no instability towards patterns and the color code indicates the most unstable longitudinal wavenumber. Fixed parameter values are indicated in Table 2. A) Froude number (h_0 fixed) vs. vegetation carrying capacity ($\alpha_g = 1\,\mathrm{m^2 s^{-1}}$, $\alpha_d = 1\,\mathrm{m^{-3}s}$, $D = 0\,\mathrm{m^2 s^{-1}}$ and $\gamma = 10^{-3}$), B) Froude number (h_0 fixed) vs. vegetation growth coefficient ($\tilde{\phi}_m = 50\,\mathrm{m^{-2}}$, $\alpha_d = 1\,\mathrm{m^{-3}s}$, $D = 0\,\mathrm{m^2 s^{-1}}$ and $\gamma = 10^{-3}$), C) Froude number (h_0 fixed) vs. vegetation uprooting coefficient ($\tilde{\phi}_m = 50\,\mathrm{m^{-2}}$, $\alpha_g = 1\,\mathrm{m^2 s^{-1}}$, $D = 0\,\mathrm{m^2 s^{-1}}$ and $\gamma = 10^{-3}$), D) Froude number (h_0 fixed) vs. sediment parameter ($\tilde{\phi}_m = 50\,\mathrm{m^{-2}}$, $\alpha_g = 1\,\mathrm{m^2 s^{-1}}$, $\alpha_d = 1\,\mathrm{m^{-3}s}$ and $D = 0\,\mathrm{m^2 s^{-1}}$).

Table 3. Fixed parameters of the 2D analysis

| Parameter name	Variable	Value	Units
Normal water depth	$\tilde{Y}_0$	1	m
Stokes drag coefficient	c_D	1.5	-
Vegetation diameter	d	0.01	m
Strickler coefficient	k_{st}	33.33	$\text{m}^{1/3}\text{s}^{-1}$
Median sediment diameter	d_{50}	0.005	m
Transverse slope parameter	r	0.5	-
Vegetation growth coefficient	α_g	1	m^2s^{-1}
Vegetation uprooting coefficient	α_d	1	m^{-3}s
Vegetation diffusion coefficient	D	100	m^2s^{-1}
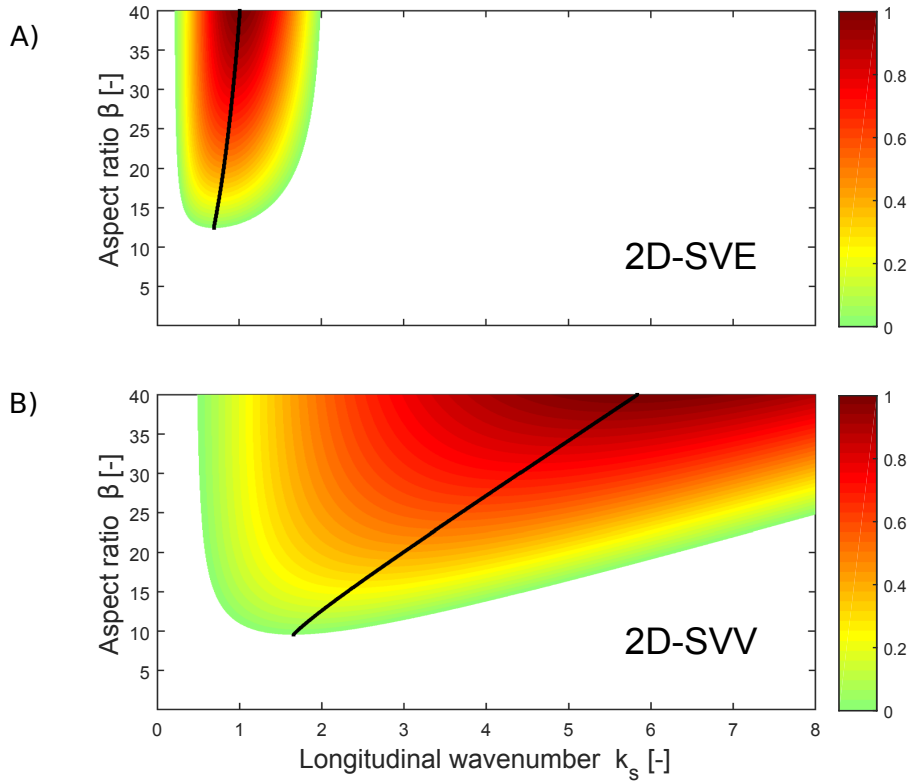
Figure 7. 2D instability domains of SVE and SVV: white means no instability towards patterns, the color code indicates the maximum exponential growth coefficient (normalized to the maximum value occurring in each figure) and the black line marks the selected longitudinal wavenumber for each aspect ratio. Fixed parameter values are indicated in Table 3. A) Longitudinal wavenumber vs. aspect ratio for alternate bars on a movable bed without vegetation ($F_0 = 0.5$ and $m = 1$), B) Longitudinal wavenumber vs. aspect ratio for alternate bars on a fixed bed with vegetation ($F_0 = 1.5$, $\tilde{\phi}_m = 50\,\mathrm{m}^{-2}$ and $m = 1$).
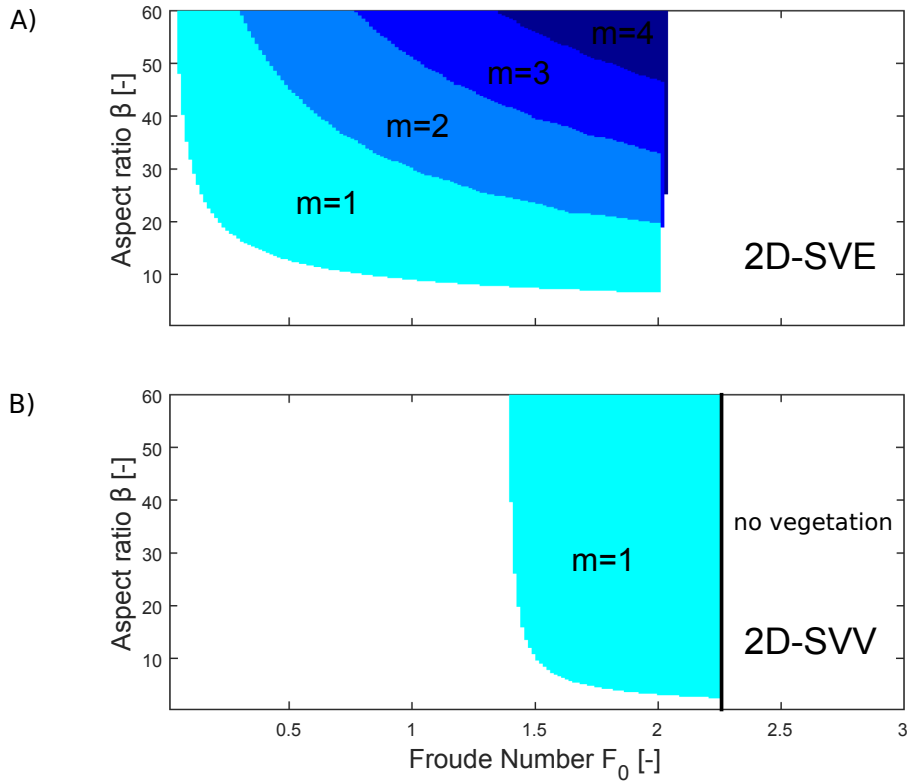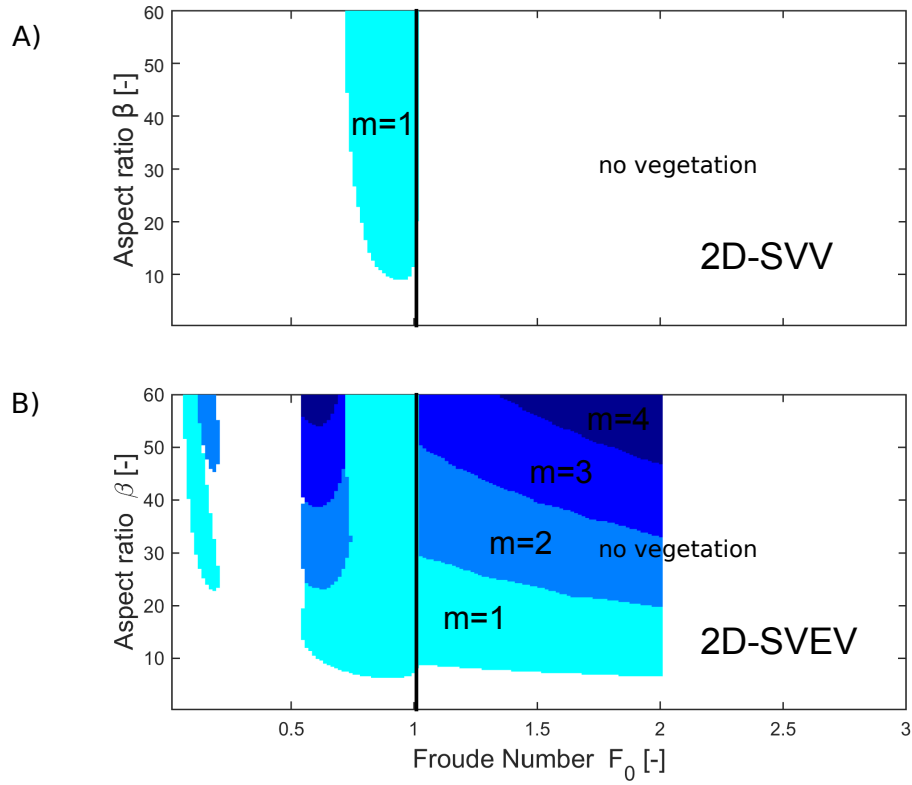
Figure 8. 2D instability domains of SVE and SVV: white means no instability towards patterns and the color code indicates bar order m. Light blue is for $m = 1$ (alternate bars) and darker blues are for $m = 2, 3, 4$ (multiple bars). No vegetation survives to the right of the black line. Fixed parameter values are indicated in Table 3. A) Froude number (h_0 fixed) vs. aspect ratio for movable bed without vegetation, B) Froude number (h_0 fixed) vs. aspect ratio for a fixed bed with vegetation ($\tilde{\phi}_m = 50 \, \mathrm{m}^{-2}$).
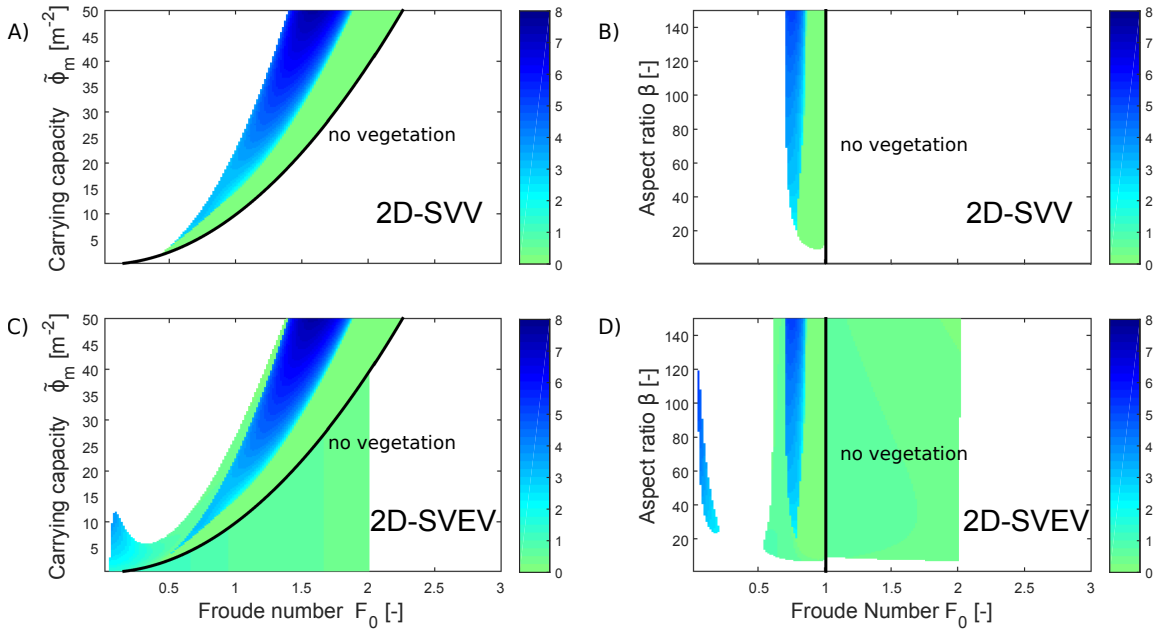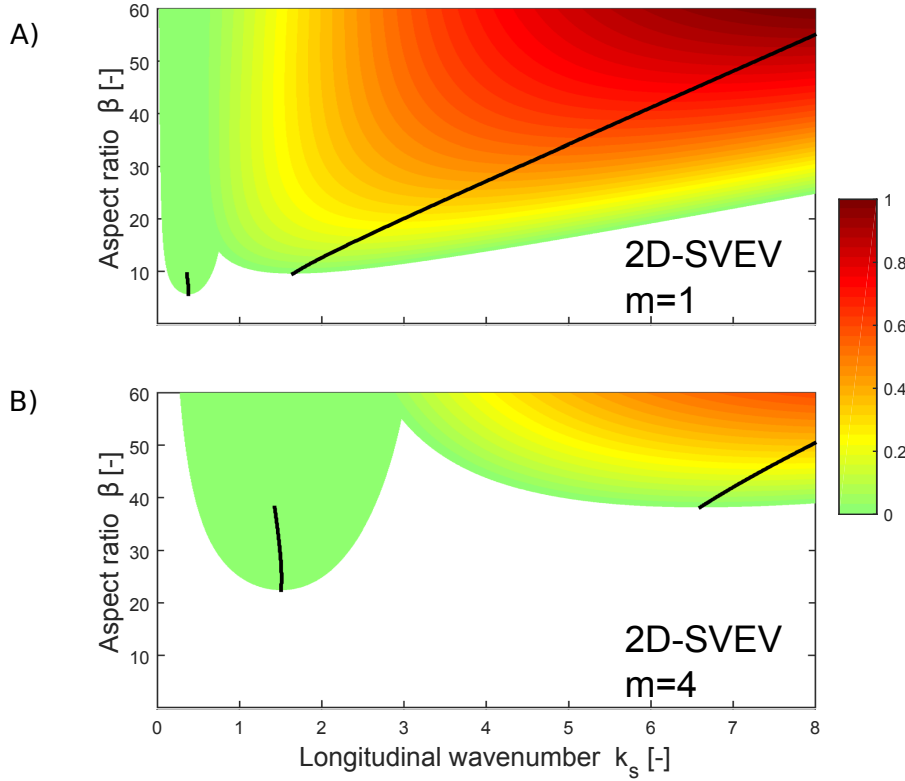
Figure 9. 2D instability domains of SVV and SVEV: white means no instability towards patterns and the color code indicates the most unstable longitudinal wavenumber. No vegetation survives to the right of the black line. Fixed parameter values are indicated in Table 3. A) Froude number (h_0 fixed) vs. vegetation carrying capacity on a fixed bed with vegetation ($\beta = 50$ and $m = 1$), B) Froude number (h_0 fixed) vs. aspect ratio on a fixed bed with vegetation ($\tilde{\phi}_m = 10\,\mathrm{m}^{-2}$ and $m = 1$), C) Froude number (h_0 fixed) vs. vegetation carrying capacity on a movable bed with vegetation ($\beta = 50$ and $m = 1$), D) Froude number (h_0 fixed) vs. aspect ratio on a movable bed with vegetation ($\tilde{\phi}_m = 10\,\mathrm{m}^{-2}$ and $m = 1$).
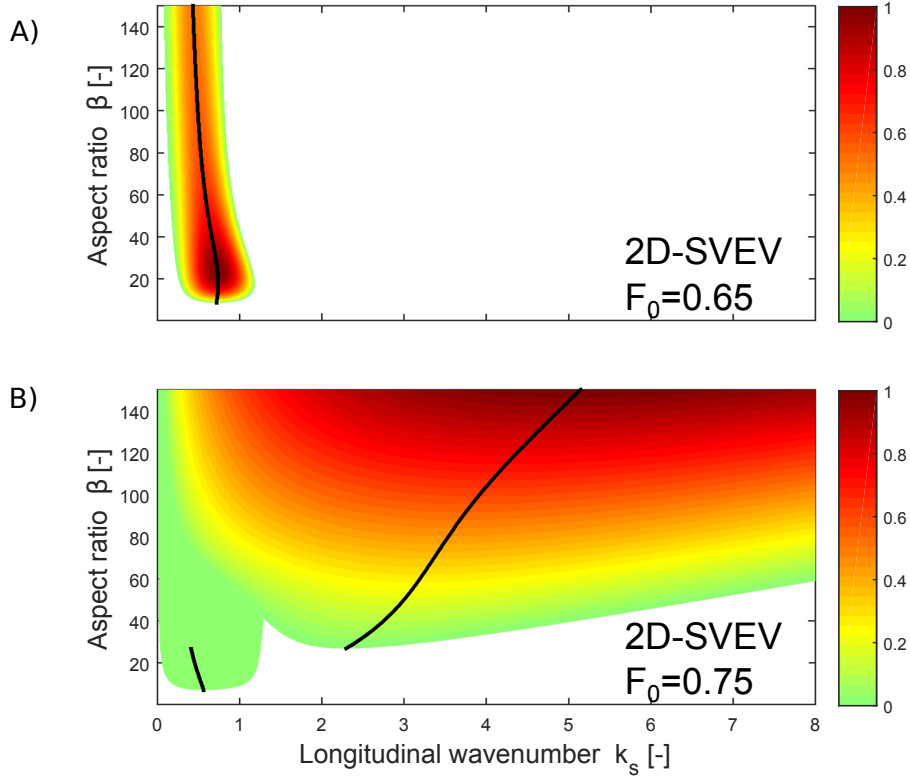
Figure 10. 2D instability domains of SVEV: white means no instability towards patterns, the color code indicates the maximum exponential growth coefficient (normalized to the maximum value occurring in each figure) and the black line marks the selected longitudinal wavenumber for each aspect ratio. Fixed parameters are indicated in Table 3. A) Longitudinal wavenumber vs. aspect ratio for alternate bar formation on a movable bed with vegetation ($\tilde{\phi}_m = 10\,\mathrm{m}^{-2}$, $F_0 = 0.65$ and $m = 1$), B) Longitudinal wavenumber vs. aspect ratio for multiple bar formation on a movable bed with vegetation ($\tilde{\phi}_m = 10\,\mathrm{m}^{-2}$, $F_0 = 0.75$ and $m = 1$).

Figure 11. 2D instability domains of SVV and SVEV: white means no instability towards patterns and the color code indicates bar order m. Light blue is for $m = 1$ (alternate bars) and darker blues are for $m = 2, 3, 4$ (multiple bars). No vegetation survives to the right of the black line. Fixed parameter values are indicated in Table 3. A) Froude number (h_0 fixed) vs. aspect ratio for fixed bed with vegetation ($\tilde{\phi}_m = 10\,\mathrm{m}^{-2}$), B) Froude number ($h_0$ fixed) vs. aspect ratio for movable bed with vegetation ($\tilde{\phi}_m = 10\,\mathrm{m}^{-2}$).

Figure 12. 2D instability domains of SVEV: white means no instability towards patterns, the color code indicates the maximum exponential growth coefficient (normalized to the maximum value occurring in both figures) and the black line marks the selected longitudinal wavenumber for each aspect ratio. Fixed parameters are indicated in Table 3. A) Longitudinal wavenumber vs. aspect ratio for alternate bar formation on a movable bed with vegetation ($\tilde{\phi}_m = 50\,\mathrm{m}^{-2}$, $F_0 = 1.5$ and $m = 1$), B) Longitudinal wavenumber vs. aspect ratio for alternate bar formation on a movable bed with vegetation ($\tilde{\phi}_m = 50\,\mathrm{m}^{-2}$, $F_0 = 1.5$ and $m = 4$).